

Formation of Icosahedral Al(Mn) by Directed Energy Processes

J. A. Knapp and D. M. Follstaedt

Sandia National Laboratories, Albuquerque, New Mexico 87185

(Received 25 June 1985)

Surface layers of icosahedral $\text{Al}_{84}\text{Mn}_{16}$ have been formed for the first time by ion-beam mixing of deposited Al/Mn layers on Al substrates at $\sim 80^\circ\text{C}$ and by either of two rapid electron-beam heat treatments of such layers. The well-defined temperature histories allow us to place limits on the melting point ($660^\circ\text{C} < T_m < 930^\circ\text{C}$) and the time needed for nucleation of the icosahedral phase from the melt at 660°C ($\tau_n < 900$ ns). The microstructures observed place restrictions on a proposed microtwinning structural model.

PACS numbers: 61.80.Jh, 61.50.Cj, 61.55.Hg

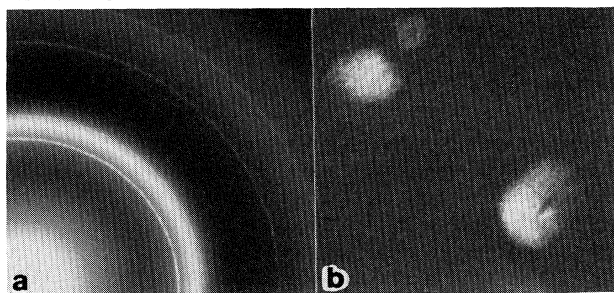
Within the past year, electron diffraction examination of melt-quenched Al(Mn) has revealed a phase exhibiting icosahedral orientational symmetry,^{1,2} which is inconsistent with invariance under lattice translation. Microtwinned rhombohedral cells can reproduce the observed symmetries of electron diffraction patterns for this phase,² but the evidence for such twinning in this case has been questioned.^{1,3,4} Penrose tiling with two cellular units which form a "quasicrystal" with icosahedral symmetry has been proposed,⁵ and appears to be in agreement with observed high-resolution transmission-electron-microscopy (TEM) images.^{3,4} If the latter explanation is correct, then quasicrystals are a new class of ordered structure which has long-range orientational order but lacks translational symmetry. The thermodynamic properties of this metastable phase and the exploration of other techniques which lead to its formation are thus of considerable interest.

We have formed thin surface layers of the icosahedral phase of Al(Mn) by three different surface alloying techniques, collectively referred to as "directed energy processes." The first of these is ion-beam mixing, in which bombardment of Al/Mn layers on an Al substrate with a Xe ion beam to a sufficient fluence at $T \sim 80^\circ\text{C}$ directly forms the icosahedral phase without a separate thermal treatment. We believe that this and the accompanying Letter by Lilienfeld *et al.*⁶ are the first reports of its formation by ion-beam mixing, which is quite different from melt quenching. The other two alloying techniques involve rapid heating of the surface region with two different electron-beam systems in different time regimes. Although generally analogous to other liquid-quenching techniques, such as melt spinning, which have been used previously to form the icosahedral phase, the two electron-beam treatments have well-defined thermal histories which allow us to place limits on the melting point of the icosahedral phase and on the time needed for nucleation of the phase. The microstructures produced by these methods are fine grained and produce ring-diffraction patterns; these features place restrictions on the microtwinning model.

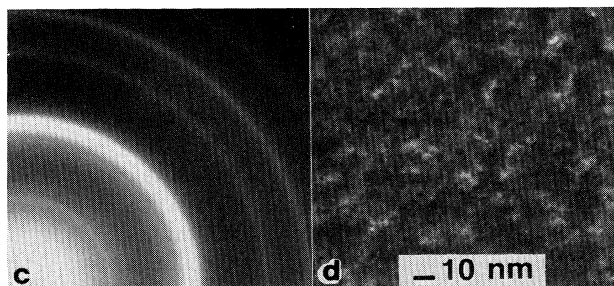
The Al(Mn) alloys were prepared on electropolished Al substrates, either $\langle 110 \rangle$ single crystals or polycrystalline disks of $\sim 500\text{-}\mu\text{m}$ thickness, by vapor deposition of alternating Al/Mn layers in a vacuum of 5×10^{-7} Torr. A typical sample used eight layers of ~ 16.4 nm of Al and eight layers of ~ 2.3 nm of Mn for a total thickness of ~ 150 nm. Integrated areal densities of carbon and oxygen across the deposited films were measured by nuclear-reaction analysis to be ~ 1.7 and $\sim 3.5 \times 10^{16}$ atoms/cm², respectively. This oxygen level is equivalent to ~ 5 nm of Al_2O_3 . The deposited layers were irradiated with 400-keV Xe ions to fluences of 2, 5, or 10×10^{15} Xe/cm² at $T \sim 80^\circ\text{C}$. The highest resulting Xe concentration is ~ 1 at.% and peaks just below the deposited layers. The chemically inert Xe is not believed to participate in the metastable-alloy formation, but produces two effects important to the sample preparation: (1) intermixing of the Al/Mn layers to form a homogenous alloy, and (2) improvement of the alloy layer adhesion to the substrate during subsequent electron-beam heat treatments.

Samples for examination by TEM were prepared by jet electropolishing from the untreated side of the substrate. In all samples, a surface layer of uniform thickness containing Al and Mn was observed in the thin areas, with ample dimensions ($> 50 \mu\text{m}$) for TEM analysis at 120 keV. The layers showed ring diffraction patterns which were readily distinguishable from fcc Al spot patterns because of the substrate in thicker areas; the latter provided an internal reference ($a_0 = 0.405$ nm) for measurement of the planar spacings of the rings. Examination with TEM of as-deposited layers showed sharp Al rings and a broader ring with $d = 0.1213$ nm, which is near the position of the brightest ring of $\alpha\text{-Mn}$ (0.210 nm). After mixing with 2×10^{15} Xe/cm², the same rings are again observed, as shown in Fig. 1(a). Dark-field imaging with the 0.213-nm ring and with the (111) and (200) Al rings on either side of it illuminated grains typically 20 nm in diameter, with some up to 40 nm, as shown in Fig. 1(b). It is clear that Al and Mn have not completely reacted with each other after the low Xe flu-

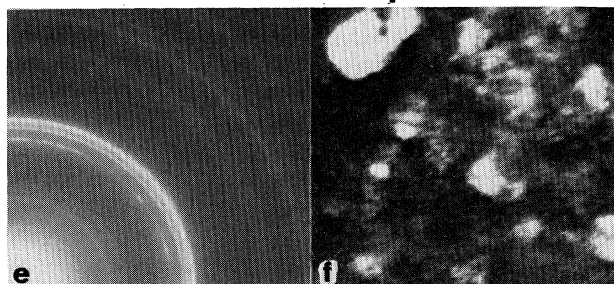
$2 \times 10^{15} \text{ Xe/cm}^2$



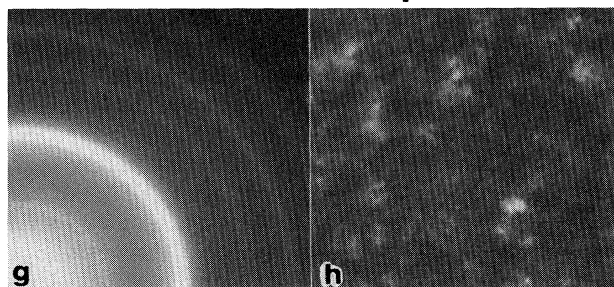
$10 \times 10^{15} \text{ Xe/cm}^2$



$2 \times 10^{15} \text{ Xe/cm}^2 + \text{LEBA}$



$2 \times 10^{15} \text{ Xe/cm}^2 + \text{PEBA}$



▲ ▲ ▲ ▲

FIG. 1. Electron diffraction patterns and dark-field images showing grain sizes for the individual treatments of $\text{Al}_{84}\text{Mn}_{16}$ surface alloys on Al. The printing of the diffraction patterns was adjusted to show rings of differing intensities. Arrows at the bottom mark the positions of rings due to the icosahedral phase.

ence. After mixing with $10 \times 10^{15} \text{ Xe/cm}^2$, the (111) Al ring is barely detectable, but new rings were found as shown in Fig. 1(c). The d spacings of these rings are the same as those observed with the electron-beam methods; average values obtained with all treatments for 16 at.% Mn are given in Table I. Also listed are the more intense reflections observed with x-ray diffraction from the icosahedral phase in melt-spun material; Bancel *et al.*⁷ indexed all their reflections with a model based on icosahedral symmetry. The agreement is excellent, and thus we identify the phase produced by our treatments as the icosahedral phase. Dark-field imaging with use of the two brightest rings ($d = 0.217, 0.206 \text{ nm}$) shows many fine grains ($\sim 10 \text{ nm}$) of the icosahedral phase [Fig. 1(d)]. Analysis with Rutherford backscattering spectroscopy showed a uniform Mn concentration of $16 \pm 1 \text{ at.}\%$ across the layers, with no significant mixing into the substrate.

Ion-beam mixing for these samples was performed without deliberate sample heating. Subsequent experiments allow us to infer a temperature of $\sim 80^\circ\text{C}$ during irradiation due to heating by the $0.5\text{-}\mu\text{A}$ 400-keV Xe beam; mixing at 60°C produces an amorphous phase, while mixing at 100°C results in a larger-grained icosahedral layer. This dependence on sample temperature suggests that the icosahedral phase does not form within the dense ion cascade, but rather during subsequent defect evolution.

The first of the two electron-beam treatments used a line-source electron-beam annealer (LEBA), which supplies a sheet beam focused to $1 \text{ mm} \times 2 \text{ cm}$.⁸ Sam-

TABLE I. Diffraction peaks from icosahedral Al(Mn).

Electrons ^a		X rays ^b	
d (nm)	Intensity	d (nm)	Intensity
0.388(5)	m	0.385	22
0.335(4)	w	0.335	8
0.254(4)	w ^c	0.252	3
0.238(4)	w ^c	0.238	...
0.218(2)	s	0.217	100
0.207(2)	s	0.2065	78
0.150(1)	m	0.1496	11
0.146(1)	vw	0.1459	3
0.128(1)	m	0.1275	20
0.109(1)	w ^d	0.1101	5
		0.1085	7
0.090(1)	vw

^aUncertainty in the last decimal place is given in parentheses. Intensities: strong (s), medium (m), weak (w), and very weak (vw).

^bFrom Ref. 7; includes all reflections of which $I \geq 3$.

^cResolved after LEBA treatment of a sample mixed with $1 \times 10^{16} \text{ Xe/cm}^2$ (not shown in Fig. 2).

^dBroad ring, possibly two unresolved rings.

ples were swept under the electron beam at speeds of ~ 180 cm/s, which has the same effect as exposure of the treated area to a broad beam with a ~ 550 μ s FWHM dwell time. The thermal history of the sample can be accurately calculated with use of finite-element methods; similar methods have been used to calculate thermal histories for Si and 304 stainless steel and give good agreement with experimental observations.^{8,9} In Fig. 2(a), the calculated temperature history shows the surface alloy reaching 660 °C, the melting point of the Al substrate, and staying there for ~ 200 μ s. The temperature rises only a few degrees at most above 660 °C; the thermal gradient across the surface layer is negligible. After the substrate recrystallization front has returned to the surface, the surface alloy cools at a rate of $\sim 7 \times 10^5$ K/s, which is comparable to melt-spinning quench rates.

The LEBA treatment was applied to a sample mixed with 2×10^{15} Xe/cm², whose layers consisted primarily of unreacted metals. Optical microscopy of the surface revealed features exhibiting flow, confirming that the substrate had melted. Analysis with Rutherford backscattering spectroscopy showed no significant change in the Mn profile; however, the Xe profile had been

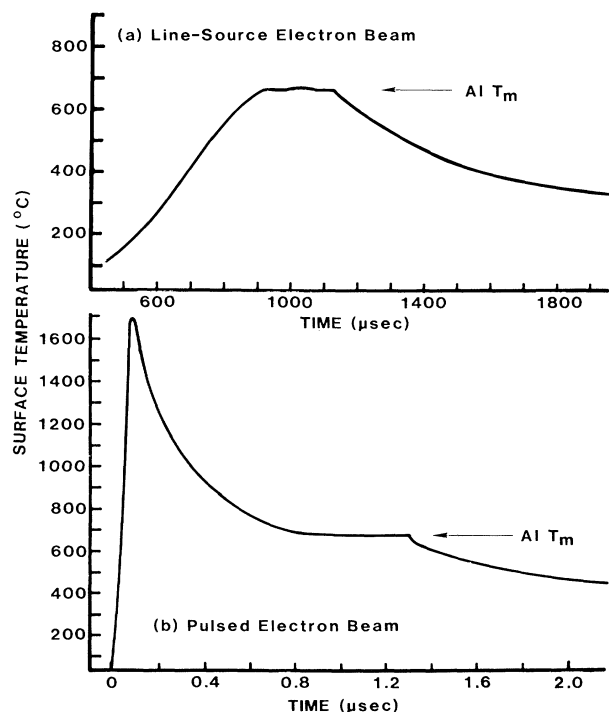


FIG. 2. Surface-temperature histories calculated for the two electron-beam treatments. (a) LEBA treatment with 38.5 keV, 75 kW/cm², and a sweep speed of 184 cm/s for a Gaussian FWHM dwell time of 543 μ s. (b) PEBA treatment with a 92-ns pulse, and total deposited energy of 2.4 J/cm².

zone refined from an initial distribution extending to ~ 0.3 μ m to a depth corresponding to the Al/Al(Mn) interface at 0.15 μ m, which also indicates that melting has occurred. Xenon being blocked from reaching the surface implies that the alloy layer had solidified before the Xe which was moving with the liquid-solid interface reached it. Examination of the alloy layer with TEM revealed the icosahedral ring pattern plus Al rings, as shown in Fig. 1(e). The random orientation of the grains is taken to indicate that nucleation occurred within the liquid phase. Dark-field imaging with the two brightest rings showed grains 10–50 nm in diameter, as seen in Fig. 1(f), but these may include some fcc Al. The grains observed after the LEBA treatment are larger and more distinct than those obtained after ion-beam mixing, but are much smaller than those observed by splat quenching of liquids from higher temperatures (~ 2 μ m).^{1,2} The small grain sizes imply a high nucleation density ($\sim 10^{17}$ /cm³), which we interpret to mean that the liquid from which the grains nucleated was highly undercooled with respect to the melting point (T_m) of the icosahedral phase; thus $T_m > 660$ °C. Taking the melting point of this phase to be less than the Al-Mn liquidus at 16 at.% Mn,¹⁰ we obtain 660 °C $< T_m < 930$ °C.

The second of the two electron-beam heating techniques used a pulsed electron-beam annealer (PEBA)¹¹ to treat another sample mixed with 2×10^{15} Xe/cm² with a 92-ns pulse of electrons, depositing a total of 2.4 J/cm². The calculated surface temperature history is shown in Fig. 2(b). The temperature reached ~ 1700 °C within 80 ns, and the sample melted to a depth of 4 μ m. The quench rate at the surface while the sample was cooling to the melting point of Al was $\sim 0.9 \times 10^9$ K/s, which is much faster than the rates attained in melt spinning. Examination with optical microscopy revealed surface-flow features which were indicative of a melt; Rutherford backscattering analysis showed a flattening of the Mn profile, but no appreciable diffusion into the substrate. Examination with TEM showed that the icosahedral phase was again present, with grains 10–30 nm [Figs. 1(g) and 1(h)]. The fine grain size again argues that $T_m > 600$ °C, as with the LEBA treatment. The time spent in the liquid phase below 930 °C places an upper limit of $\tau_n < 900$ ns on the time needed for nucleation of the icosahedral phase; for much of this time the temperature was near 660 °C.

The microstructures observed here place restrictions on the model involving microtwinning with a rhombohedral unit cell,² where multiple diffraction is used to produce reflections in the fivefold symmetric pattern at diffraction angles and apparent planar spacings not found for the rhombohedral crystal. This model would require that each grain contain several of the twin variants; multiple diffraction among randomly

oriented grains would not produce the effect. Such microtwinning would then have to occur within grains < 40 nm, perhaps as small as ~ 10 nm. As a further consideration, the x-ray-diffraction study of Bancel *et al.*⁷ shows that they observe all the reflections seen in TEM examinations of single icosahedral grains. The ring patterns in Fig. 1 contain all of the more intense reflections seen with x-ray diffraction, and among those reflections the relative intensities agree, as indicated in Table I. This agreement suggests that our individual grains contain essentially the full icosahedral symmetry, and for this to be true, most of the twenty twin variants would have to coexist in each grain. Twinning on this fine scale would appear to be a significant constraint for this model.

The microstructure resulting from the LEBA treatment shows no evidence of other Al-Mn compounds. Thus the icosahedral phase with 16 at.% Mn not only nucleates preferentially from the liquid, but is also stable against transformation to other phases for at least 200 μ s at 660 °C. Furthermore, with *in situ* heating in the TEM, the free-standing polycrystalline layers did not transform to another phase until the 10-min anneals at 50 °C increments reached 450 °C. The transformation occurred at 350 °C, however, in areas where the icosahedral layer was still in contact with the fcc Al substrate. Thus icosahedral Al(Mn) is relatively stable against solid-state transformation.

The ion-beam mixing and PEBA experiments discussed here for Al(Mn) are similar to studies on Al(Ni).^{12,13} In PEBA treatments of Al(Ni) surface alloys on Al, the compound Al₃Ni (which has a relatively large orthorhombic unit cell) did not nucleate from the liquid, but AlNi (which has a simpler, CsCl structure) did form. The absence of Al₆Mn, which has a large orthorhombic unit cell, in the present work is consistent with this result. On the other hand, the icosahedral phase is able to nucleate within at most 900 ns, despite its presumably complicated overall structure. This may be a result of relatively simple structural units being arranged into a Penrose framework. It would appear to be more difficult to nucleate a rhombohedral cell with numerous twin variants simultaneously present. The icosahedral phase has

been observed for a series of 3d transition elements alloyed into Al: Cr, Mn, and Fe^{1,2}; however, it was not observed in the Al(Ni) experiments. The similarity of results obtained with ion-beam mixing and ion implantation in Al(Ni)¹² leads us to predict that icosahedral Al(Mn) will be formed by implanting Mn into Al at ~ 100 °C.

Technical assistance by G. L. Schuh and M. P. Moran is gratefully acknowledged. This work was supported by the Department of Energy through Grant No. DE-AC04-76-DP00789.

¹D. Shechtman, I. Blech, D. Gratias, and J. W. Cahn, *Phys. Rev. Lett.* **53**, 1951 (1984).

²R. D. Field and H. L. Fraser, *Mater. Sci. Eng.* **68**, L17 (1984).

³R. Gronsky, K. H. Krishnan, and L. Tanner, in *Proceedings of the Forty-Third Annual Meeting of the Electron Microscopy Society of America*, edited by G. W. Bailey (San Francisco Press, San Francisco, 1985), kp. 34.

⁴D. Shechtman, D. Gratias, and J. W. Cahn, *C.R. Seances Acad. Sci., Ser. 2* **300**, 909 (1985).

⁵D. Levine and P. J. Steinhardt, *Phys. Rev. Lett.* **53**, 2477 (1984).

⁶D. A. Lilienfeld *et al.*, preceding Letter [*Phys. Rev. Lett.* **55**, 1587 (1985)].

⁷P. A. Bancel, P. A. Heiney, P. W. Stephens, A. I. Goldman, and P. M. Horn, *Phys. Rev. Lett.* **54**, 2422 (1985).

⁸J. A. Knapp and S. T. Picraux, *J. Appl. Phys.* **53**, 1492 (1982); J. A. Knapp, *J. Appl. Phys.* (to be published).

⁹S. T. Picraux, J. A. Knapp, and M. J. Davis, *J. Nucl. Mater.* **120**, 278 (1984).

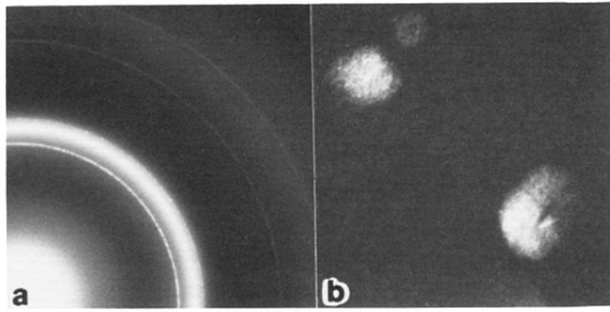
¹⁰*Metals Handbook* (American Society of Metals, Metals Park, Ohio, 1973), 8th ed., Vol. 8, p. 262.

¹¹J. A. Knapp and D. M. Follstaedt, *Mater. Res. Soc. Symp. Proc.* **4**, 407 (1982).

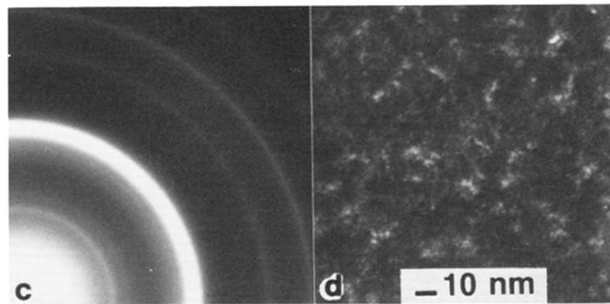
¹²D. M. Follstaedt, *Nucl. Instrum. Methods B* **7/8**, 11 (1985).

¹³D. M. Follstaedt, S. T. Picraux, P. S. Peercy, J. A. Knapp, and W. R. Wampler, *Mater. Res. Soc. Proc.* **28**, 273 (1982), and in *Alloy Phase Diagrams* edited by L. H. Bennett, B. C. Giespen, and P. B. Massalski (Materials Research Society, Pittsburgh, 1984), p. 94.

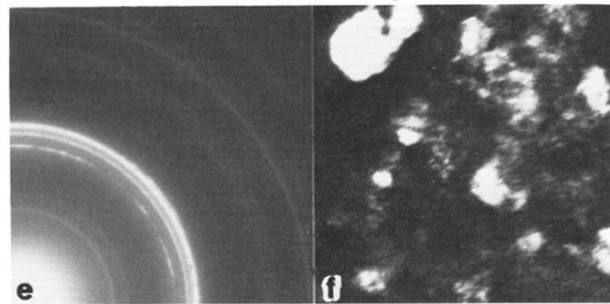
$2 \times 10^{15} \text{ Xe/cm}^2$



$10 \times 10^{15} \text{ Xe/cm}^2$



$2 \times 10^{15} \text{ Xe/cm}^2 + \text{LEBA}$



$2 \times 10^{15} \text{ Xe/cm}^2 + \text{PEBA}$

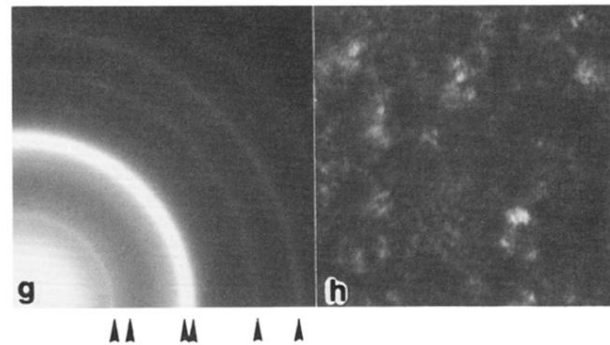


FIG. 1. Electron diffraction patterns and dark-field images showing grain sizes for the individual treatments of $\text{Al}_{84}\text{Mn}_{16}$ surface alloys on Al. The printing of the diffraction patterns was adjusted to show rings of differing intensities. Arrows at the bottom mark the positions of rings due to the icosahedral phase.